ADVANCED FUNCTIONAL MATERIALS
www.afm-journal.de

LipoGels: Robust Self-Lubricating Physically Cross-Linked Alginate Hydrogels Embedded with Liposomes

*Tao Ma, Xueying Guo, Najet Mahmoudi, Pierangelo Gobbo, and Wuge H. Briscoe**

The exceptional lubricity in living systems has stimulated wide scientific interest in the design of biomimetic lubricants. Here, a sodium alginate hydrogel physically cross-linked with divalent cations (Ca^{2+}), incorporating ≈100 nm 1,2-dipalmitoyl-*sn*-glycero-3-phosphocholine liposomes in trace amounts (≈0.004–0.08 wt% lipids), which are termed "LipoGels", is optimized to overcome gelation shrinkage to generate a homogeneous and smooth surface. Cryogenic scanning electron microscopy reveals the compact porous gel structure with embedded liposomes, and confocal fluorescent microscopy reveals a uniform distribution of liposomes in the gel. The LipoGels demonstrate robust mechanical strength, with an elastic modulus G' > 200 kPa and a Young's modulus E ≈1 MPa from rheology and microindentation measurements, respectively. Small-angle neutron scattering deduces a classic de Gennes' mesh size of ξ ≈3.8 nm for the polymer network, consistent with that estimated from the rheology results. The underwater friction coefficient of liposome–alginate hybrid LipoGels, evaluated in the sphere-on-flat geometry with a tribometer, is as low as μ ≈0.02 at a maximum contact pressure of 0.45 MPa. These results offer nanostructural insights into the hybrid liposome–alginate hydrogels, prepared by facile physical cross-linking, demonstrating their potential as biomimetic lubricants, also with encapsulation capacities for functional additives.

1. Introduction

The ultralow friction devised by living systems (e.g., knee joints and eyelids), with a friction coefficient (CoF) as low as μ ≈0.001[1] at physiological pressures of tens of MPa,[2] has stimulated intensive research into mimicking such extraordinary lubrication and investigating underlying mechanisms.[3] Articular cartilage, a complex biohydrogel covering the end bone of a joint,[4] plays a crucial role in facilitating ultralow joint friction, where hyaluronan (HA), aggrecans, lubricins, and phospholipids synergistically form the robust lubricating boundary layer to dissipate energy upon sliding[5] via the fundamental mechanism of hydration lubrication.[6] The molecular origin of such efficacy arises from the load-bearing capacity of water molecules tenaciously bound to the charged and zwitterionic groups in the biomacromolecules and lipids,[7] while retaining fluidity and facilitating frictionless sliding.

Among the components constituting the cartilage boundary layer, the highly hydrated zwitterionic head groups of phospholipids present at the cartilage surface and in the synovial fluid[8] are central to mediating the hydration lubrication mechanism.[9] Several lubricating systems have been successfully designed utilizing this property, including lipid bilayers, liposomes, and HA–liposome hybrids.[6b] Very recently, a novel strategy has emerged, incorporating liposomes in hydrogels for designing biomedically suited lubricating materials.[10]

Hydrogels are dual- or multicomponent systems with water confined in a 3D hydrophilic polymer network.[11] With robust mechanical strength, biocompatibility, high water content, and multifunctionality,[12] hydrogels have been explored as candidates for articular cartilage replacements.[13] It however remains challenging to prepare lubricating hydrogels with mechanical robustness and biocompatibility.[14] To this end, several complex hydrogel systems have been recently proposed, including double network hydrogels,[15] nanocomposite hydrogels,[16] and layered hydrogels,[17] progressing from earlier development such as polyvinyl alcohol (PVA) hydrogels.[18] In a recent pioneering work, Lin et al. incorporated lipid multilamellar vesicles (MLVs) in synthetic hydrogels to facilitate cartilage-like lubrication.[16] The sophisticated and complex synthesis involved mixing a low concentration of liposomes of 1,2-dimyristoyl-*sn*-glycero-3-

T. Ma, X. Guo, W. H. Briscoe
School of Chemistry
University of Bristol, Cantock's Close
Bristol BS8 1TS, UK
E-mail: wuge.briscoe@bristol.ac.uk
N. Mahmoudi
ISIS Neutron and Muon Spallation Source
STFC Rutherford Appleton Laboratory
Oxfordshire OX11 0QX, UK
P. Gobbo
Department of Chemical and Pharmaceutical Sciences
University of Trieste, and INSTM Research Unit of Trieste
Via L. Giorgieri 1, Trieste 34127, Italy

The ORCID identification number(s) for the author(s) of this article can be found under https://doi.org/10.1002/adfm.202514611

DOI: 10.1002/adfm.202514611

phosphatidylcholine and L-α-phosphatidylcholine, hydrogenated (Soy) with a monomer solution, followed by polymerization and chemical cross-linking to form the hybrid hydrogel. The bulk hydrogel exhibited very low friction ($\mu \approx 0.01$) and good load-bearing capacity (with a storage modulus $G' \approx 70$ kPa), with the self-renewal property facilitated by the lipids. The hydrogels in these previous studies were chemically cross-linked, typically needing sophisticated synthesis and preparation procedures with a multitude of chemicals, which would also require additional care to minimize cytotoxicity.

In this context, physically cross-linked hydrogels facilitated by noncovalent interactions, such as electrostatic interactions, crystallization, or hydrogen bonding,[19] have attracted attention due to their facile preparation, biocompatibility, and potential for reversible gelation,[20] but suffer from poor mechanical strength.[21] Therefore, improving the mechanical properties of physically cross-linked hydrogels is essential to enabling their use in high-load demanding applications. A hydrogel of PVA grafted with 4-methyl benzaldehyde prepared by the solvent replacement in a dimethyl sulfoxide–water mixture achieved a high tensile strength of ≈3.26 MPa.[22] However, its lubrication was relatively modest with $\mu \approx 0.11$ against a stainless-steel ball, with chemicals used in the complex method also presenting biosafety risks. Hitherto, it remains a challenge to develop facile hydrogel preparation, using minimal chemicals and ensuring biocompatibility and sustainability.

Alginic acid, a polysaccharide extracted from brown algae,[23] can be physically cross-linked in its sodium salt form by certain divalent and trivalent cations, particularly Ca^{2+}, due to the presence of carboxylate groups on the polymer chain.[24] Alginate hydrogels have usually been prepared as beads or microgels for drug delivery owing to their biocompatibility, physiological stability, and facile gelation.[25] Bulk alginate hydrogels, however, are prone to shrinkage upon cross-linking in polar solvents,[26] causing ill-defined morphologies and properties, which have limited their application. In an attempt to address such gelation shrinkage, a two-step cross-linking process was developed, involving first weak cross-linking with a 50 mM $CaCl_2$ solution and subsequent molding and immersion in a 4 M $CaCl_2$ solution for 24 h.[27] However, the mechanical strength of the obtained gel was relatively low with an elastic modulus $G' < 50$ kPa. In an attempt to enhance the stiffness of alginate hydrogels, another two-step method has been proposed: a weak pregel attached to a substrate was first dried/shrunk in air, followed by further cross-linking and rehydration in a cationic solution, yielding a stiff Ca^{2+}–alginate gel with a tensile stress of ≈8 MPa.[28] However, the shrinking issue remained unresolved, with a relatively low water content of ≈60% in the final gel.

In this study, to address gelation shrinkage and mechanical weakness, important for the feasibility of alginate gels as sustainable lubricating materials, we have devised a simple method to produce a homogenous and transparent hydrogel by physical cross-linking sodium alginate solution with Ca^{2+}. The shrinkage issue was resolved, rather simply, by concentrating the sodium alginate solution through controlled evaporation before cross-linking, as detailed in Section 2.1 below. The gel was further functionalized by incorporating ≈100 nm 1,2-dipalmitoyl-*sn*-glycero-3-phosphocholine (DPPC) liposomes, confirmed by cryogenic scanning electron microscopy (cryo-SEM) and confocal fluorescence microscopy. The hybrid gel retained a high-water content, and the robustness of gel mechanical properties was characterized using microindentation and rheology, with the gel nanostructure probed with small-angle neutron scattering (SANS). Such homogenous and robust hybrid gels prepared via a simple method, which we term "LipoGels", facilitated excellent lubrication performance under water with a friction coefficient as low as $\mu \approx 0.02$ under a pressure of 0.45 MPa, demonstrating their potential as sustainable aqueous lubricants also with capacities for encapsulation of actives.

2. Results and Discussion

2.1. Overcoming Gel Shrinkage in Optimized Alginate Hydrogel Synthesis

Control Ca^{2+} cross-linked alginate hydrogels prepared as reported in literature experienced shrinkage,[24,28,29] with the obtained soft hydrogels exhibiting an irregular shape with an uneven surface (an example for 2 wt% alginate cross-linked with 5 wt% Ca^{2+} shown in **Figure 1b** top; cf. also Figure S7a in the Supporting Information), a process which could not be reproduced consistently. To overcome this, several parameters were systematically varied, including the concentration of sodium alginate (c_{alg}) and Ca^{2+} (c_{ca2+}), cross-linking time (t_{cl}, i.e., the incubation time following Ca^{2+} addition before rinsing), and the addition method of the cross-linker, with an elevated c_{alg} identified as a key factor in preventing gel shrinkage. Photographic images of shrinking and nonshrinking alginate hydrogels are further compared in Figure S7 in the Supporting Information. A macroscopically homogeneous, flat, and transparent hydrogel film (Figure 1b bottom) was ultimately achieved reproducibly in a process described as follows (cf. Figure 1a). Both the control gel and LipoGel samples showed ≈70% transmittance at a wavelength of 600 nm (cf. Section S3 in the Supporting Information), confirming their transparent optical characteristics.[30] A $c_{alg} = 2$ wt% sodium alginate solution[31] (with DPPC liposomes at a designated lipid concentration c_{DPPC} added in the case of LipoGels) was concentrated by heating it in an oven slowly over 1–1.3 h at 50 °C, with the final alginate concentration readily adjusted by controlling the heating time. Furthermore, these alginate hydrogels retained their macroscopic integrity without any observable dissolution in an ethylenediaminetetraacetic acid chelator solution over the course of one week. This overcomes the difficulty associated with slow and inhomogeneous dissolution and the drastic increase in the viscosity of the alginate solution at concentrations above $c_{alg} \approx 2$ wt% ($\eta \approx 2.01$ Pa s; cf. Figure S9 in the Supporting Information). The amount of the water loss, r_w ≈70%, was identified as a minimum value to consistently produce nonshrinking hydrogels, corresponding to an alginate concentration of $c_{alg} = 6.7$ wt% (cf. Section S5 in the Supporting Information). De Gennes' scaling arguments[32] give the relationship between the osmotic pressure Π and the polymer fraction ϕ as[33] $\Pi \approx \phi^{9/4} \approx {c_{alg}}^{9/4}$. Furthermore, the mesh size, ξ, of the hydrogel (the average distance between two adjacent cross-linking points in the alginate polymer gel network is related to ϕ as $\xi \approx \phi^{-3/4}$ so that $\Pi \approx \xi^{-3}$, consistent with a denser polymer network capable of sustaining a higher osmotic pressure. Dehydration and shrinkage upon Ca^{2+}-induced gelation would effectively reduce ξ and increase

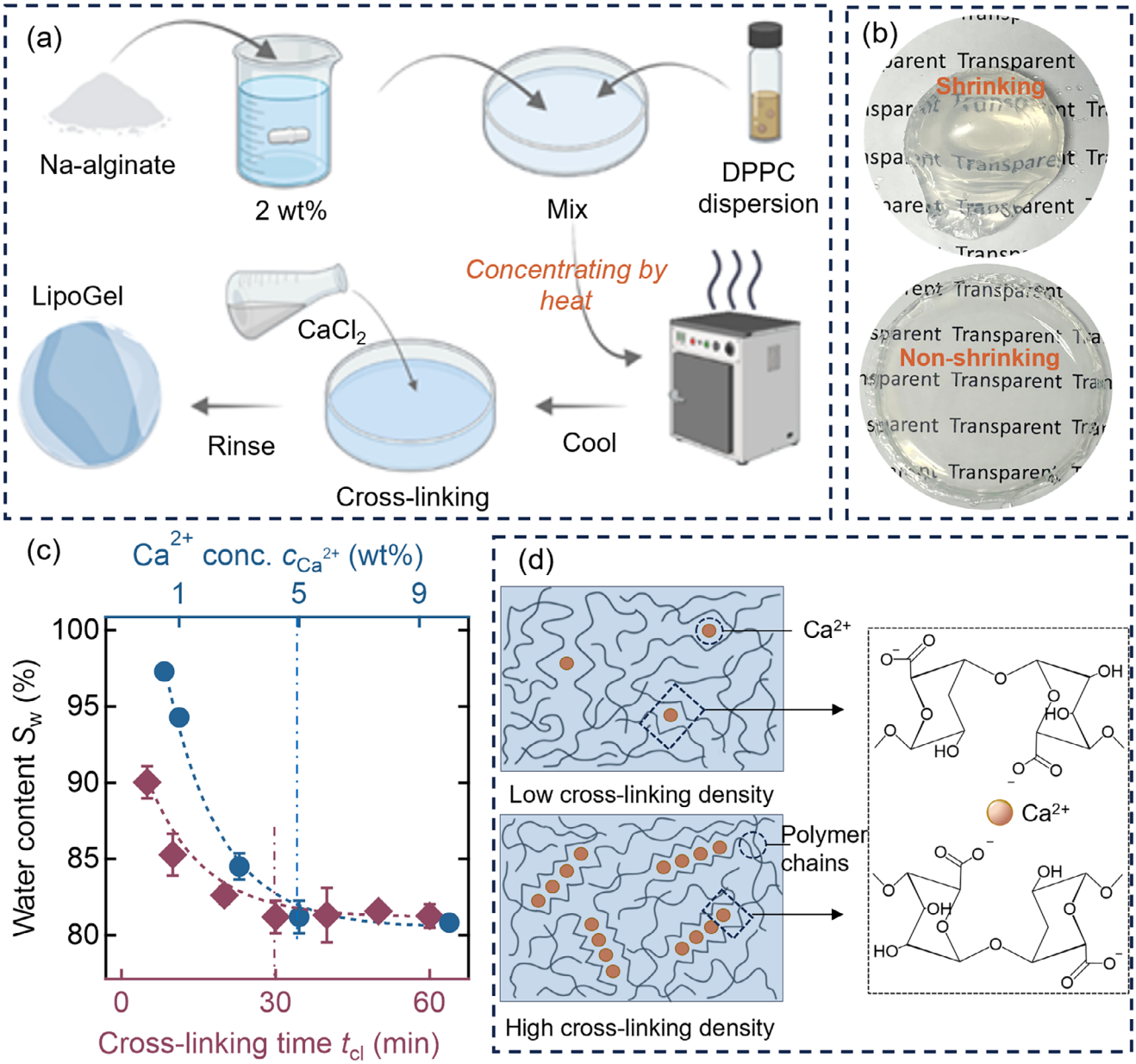

Figure 1. Preparation and optimization of nonshrinking alginate hydrogels. a) The flow chart of the LipoGel preparation method, partially created with BioRender, https://BioRender.com/wrammvm. b) Photographic images of opaque shrinking (top) and transparent nonshrinking (bottom) alginate hydrogels. c) Water content of gels, S_w, under different cross-linking times (t_{cl}, red symbols; bottom axis) and Ca^{2+} concentrations (c_{ca2+}, blue symbols; top axis), with the dashed lines a guide to the eye. d) Schematic of alginate gelation at low and high cross-linking densities and the "Egg-Box" cross-linking model.

ϕ, which thus would be countered by the internal osmotic pressure of the gelling polymer solution. By contrast, low concentration gels lack sufficient osmotic resistance, resulting in marked shrinkage. Strong hydration and a sufficiently high cross-linking density at such a high alginate concentration would sustain an internal osmotic pressure to resist dehydration and shrinkage.

The water content S_w (or swelling ratio Q, cf. Tables S1 and S2 in Section S6 of the Supporting Information) of a hydrogel is indicative of its ability to confine and retain water in the gel internal structure.[34] Here, the gel water content was measured at different Ca^{2+} concentrations c_{ca2+} and cross-linking time t_{cl} (cf. Figure 1c). First, c_{ca2+} was varied from 0.5 to 10 wt% at a cross-linking time $t_{cl} = 30$ min. As shown in Figure 1c (top axis), the water content of alginate hydrogels rapidly decreased initially before plateauing at $c_{ca2+} \approx 5$ wt%. The alginate hydrogel cross-linked at $c_{ca2+} = 0.5$ wt% showed the highest water-retaining capacity with $S_w = 97.3 \pm 0.1\%$, but appeared soft and fragile with a thickness of ≈1.3 mm. By contrast, the hydrogels cross-linked using $c_{ca2+} > 5$ wt% exhibited more robust mechanical strength, albeit with a lower water content of $S_w = 81.2 \pm 1.1\%$ and a smaller

thickness of ≈0.35 mm. Similarly, the cross-linking time was varied while c_{ca2+} was fixed at 5 wt%. For t_{cl} = 5–30 min, the water content decreased sharply from $S_w = 90.1 \pm 1.1\%$ to $S_w = 81.2 \pm 1.1\%$ (Figure 1c; lower axis), before stabilizing at S_w ≈81% at t_{cl} > 30 min. Accordingly, the optimal gelation conditions were determined as $c_{ca2+} \geq 5$ wt% and $t_{cl} \geq 30$ min when the cross-linking process reaches saturation.

The gel water content is closely related to its mechanical strength, with a lower water content usually corresponding to a higher Young's modulus.[27] A higher concentration of Ca^{2+} and a longer cross-linking time result in a higher cross-linking density. In this case, as schematically shown in Figure 1d, more carboxylate groups on alginate polymer chains are connected by chelating Ca^{2+} in the "Egg-Box" gelation model.[35] This would increase the cross-linking density and reduce the volume that water could pervade, leading to a lower swelling ratio but a more robust hydrogel.

2.2. Nanostructure of LipoGel

Cryo-SEM[36] images (**Figure 2**a,b) revealed that both LipoGel and gel (no-liposome) samples displayed similar compact porous morphologies with a dense, sponge-like internal structure, with an average pore size of ≈92 nm and a size distribution of 26–188 nm. For comparison, a minimum pore size of 24 ± 0.6 µm in a Ca^{2+}-cross-linked alginate hydrogel has been previously reported, some 260 times larger than that in this study.[37] The significantly smaller pores here resulted from the higher sodium alginate concentration prior to cross-linking, creating dense structures capable of sustaining high osmotic pressure and thus high-load applications.

Notably, spherical features attributed to liposomes were observed in the hydrogel network of the LipoGel sample (indicated by a white arrow in Figure 2b; cf. also cryo-SEM images in Figure S10 in the Supporting Information), but not in the control sample (Figure 2a), with an average diameter ≈136 nm consistent with the DLS DPPC liposome size (cf. Figure S11 in the Supporting Information). The void around the liposome in the image is likely resulting from the sublimation of its surrounding water. Cryo-SEM thus confirmed the compact porous structures of the hydrogels and the successful incorporation of DPPC liposomes.

Confocal microscopy provided high-resolution visualization of the liposome 3D-distribution within the hydrogel. In contrast to nonfluorescent control samples (cf. Figure S12 and Table S3 in the Supporting Information), only PKH67-labeled[38] DPPC liposomes showed green fluorescence in solution and when embedded in the alginate hydrogel. As shown in Figure 2d, DPPC single unilamellar vesicles (SUVs) appeared uniformly distributed throughout the hydrogel, maintaining liposome structural integrity with minimal aggregation. Measurements across multiple randomly selected hydrogel regions showed consistent, uniform fluorescent SUV distribution throughout the LipoGels (cf. Figure S13 in the Supporting Information). By contrast, large aggregates of DPPC MLVs in coexistence with smaller liposomes were visible in the gel matrix (Figure 2c) with a less uniform distribution.

The LipoGel nanostructure was evaluated using SANS (experimental details under different cross-linking conditions, including drying time t_d prior to cross-linking and DPPC liposome concentration c_{DPPC}, as well as t_{cl} and c_{ca2+}). The experimental SANS intensity profiles were fitted using the correlation length model,[39] which accounts for Porod scattering from clusters and Lorentzian scattering from polymer chains,[40] i.e.

$$I(Q) = \frac{A}{Q^n} + \frac{C}{1 + (Q\xi)^m} + \text{Background} \quad (1)$$

where I is the scattering intensity, Q the scattering vector, n and m the exponents for the Porod and Lorentzian terms, and A and C denote the respective scale factors. This yields the correlation length or mesh size, ξ, of the hydrogel (the average distance between two adjacent cross-linking points in the alginate polymer gel network;[41] cf. Figure 2h), which characterizes the hydrogel nanostructure and is intimately related to the gel mechanical properties.

As shown in Figure 2e, the SANS profiles across different DPPC lipid (and thus liposome) concentrations exhibited similar features, with the intensity decreasing linearly with Q in the low Q region, followed by plateauing towards the background asymptote, with the mesh size varying slightly in the range ξ = (3.5–4.3) ± 0.4 nm across liposome concentrations (cf. **Table 1**). This indicates that DPPC incorporation did not appreciably alter the hydrogel nanostructure. The Porod exponent, $n > 2$ for all samples (cf. Table 1), indicates that the hydrogel nanostructure could be characterized as mass fractals,[42] consistent with the previous report on gels exhibiting similar nanostructural characteristics.[43] The Lorentzian exponent (m), reflecting polymer–solvent interactions, is consistently greater than 2, suggesting that the alginate polymer chains were swollen in water,[42] with minimal interactions between monomers along the chain.[44] Overall, the SANS results indicate that DPPC liposome incorporation did not induce notable structural changes in the gel.

As shown in Figure 2f, prolonged drying prior to cross-linking led to a higher sodium alginate concentration and a reduced mesh size from $\xi = 7.6 \pm 0.5$ nm to $\xi = 2.8 \pm 0.6$ nm (with key fitting parameters listed in Table S4 in the Supporting Information), arising from a closer proximity of the polymer chains and more pronounced cross-linking of the carboxylate groups. As the drying time was increased to t_d = 90 min (with a corresponding alginate concentration of c_{alg} = 30.97 wt%), the mesh size further decreased to $\xi = 2.8 \pm 0.6$ nm. Water content S_w is a crucial consideration for lubricating hydrogels,[45] with a higher water content enhancing lubrication but weakening the gel mechanical strength. Hydrogels prepared from more concentrated sodium alginate solutions exhibited a lower S_w, reduced thickness, and enhanced mechanical strength. A drying time of t_d = 70 min in our study appeared to achieve an optimal balance.

Furthermore, the effects of cross-linking time t_{cl} and Ca^{2+} concentration c_{ca2+} were investigated under the optimized cross-linking time (t_{cl} = 30 min) and cross-linker concentration (c_{ca2+} = 5 wt%), compared to the gels prepared at t_{cl} and c_{ca2+} below and above these values. Generally, the SANS mesh sizes ξ (Figure 2g) decreased as t_{cl} and c_{ca2+} increased, attributed to higher cross-linking densities. Specifically, ξ decreased significantly from 11.7 ± 2.3 to 4.3 ± 0.4 nm as the cross-linking time increased from t_{cl} = 5 min to t_{cl} = 30 min (cf. Table S5 in the Supporting Information). However, the effect of extended t_{cl} beyond 30 min was less pronounced. Increasing the Ca^{2+} concentration from

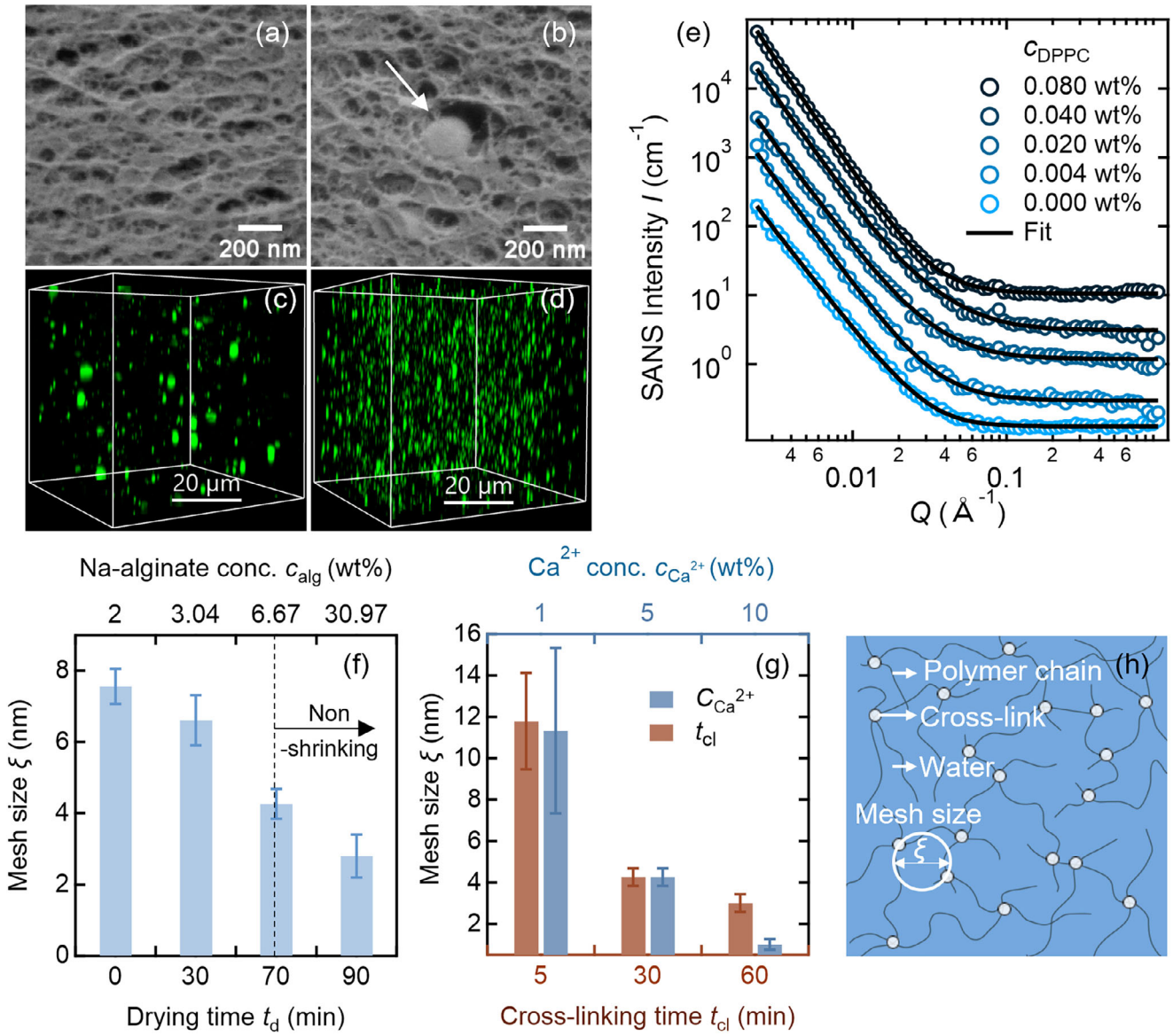

Figure 2. Nanostructural characterization of the gel (liposome-free) and LipoGel (DPPC liposome embedded). Cryo-SEM image of a) the control gel and b) LipoGel with the scale bar of 200 nm, showing the porous structures and the incorporated liposome (indicated by a white arrow in (b)). Confocal microscopy 3D image showing the distribution of PKH67 fluorescently labeled c) DPPC MLVs and d) single unilamellar vesicles (SUVs) within the LipoGel. e) SANS data (open symbols; offset on the Intensity axis for clarity) of alginate LipoGels embedded with different concentrations of DPPC SUVs, with the correlation-length fits shown as black lines. f) The gel polymer network mesh size (ξ); h) schematic from SANS fitting plotted as a function of gel drying time (bottom axis), with the corresponding alginate polymer concentration c_{alg} shown on the top axis; and g) cross-linking time t_{cl} (orange, bottom axis) and Ca^{2+} concentrations c_{Ca2+} (blue, top axis).

Table 1. SANS fitting results of alginate hydrogels embedded with different concentrations of DPPC lipids/liposomes.

DPPC conc. c_{DPPC} [wt%]	Porod exponent n	Lorentz exponent m	Mesh size ξ[nm]	Fitting error X^2
0.080	3.18 ± 0.02	2.15 ± 0.32	3.6 ± 0.7	1.35
0.040	3.06 ± 0.03	2.01 ± 0.10	3.9 ± 0.4	1.30
0.020	2.86 ± 0.03	2.00 ± 0.08	3.5 ± 0.4	1.22
0.004	2.95 ± 0.03	2.00 ± 0.56	3.6 ± 0.3	1.04
0.000	2.77 ± 0.03	4.53 ± 0.76	4.3 ±0.4	1.01

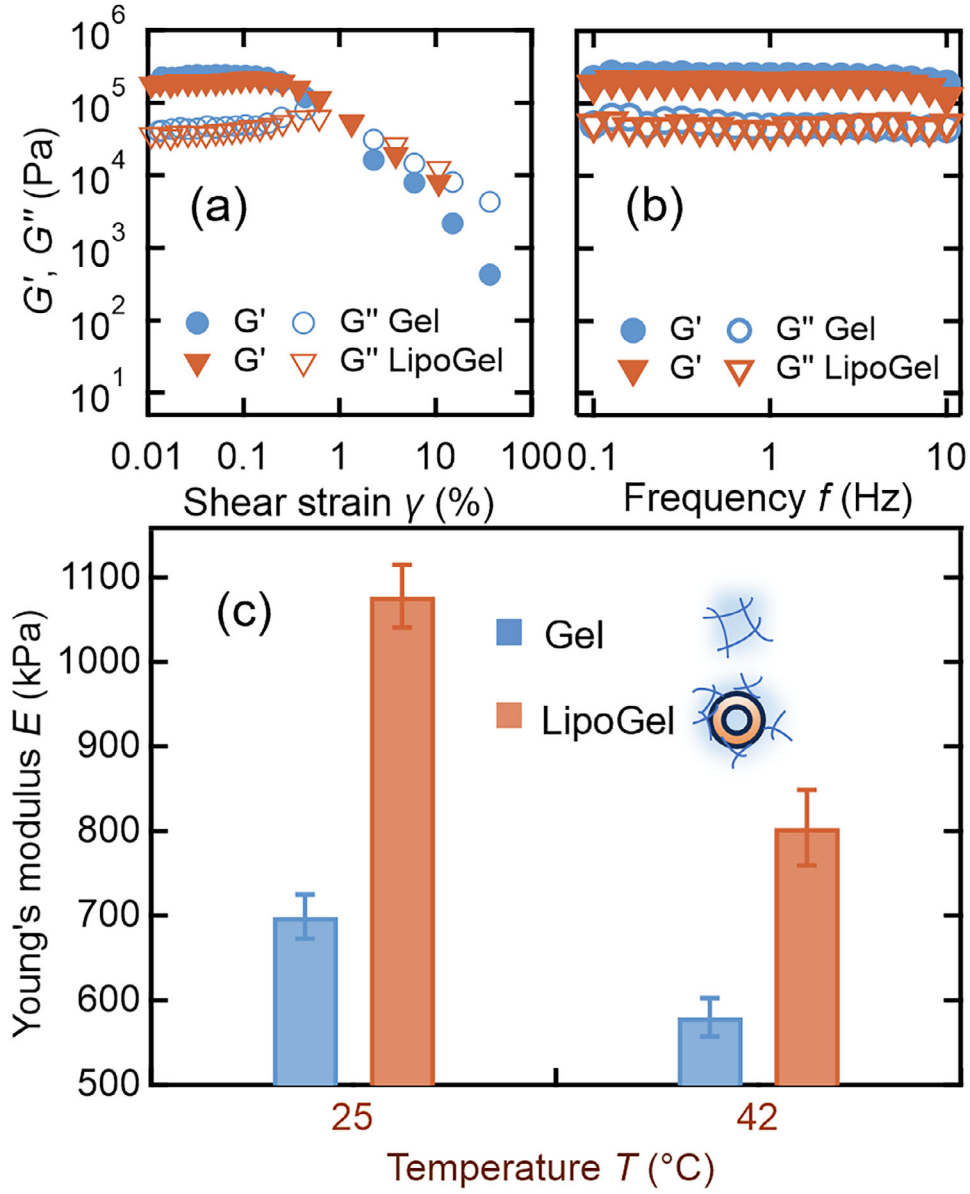

Figure 3. Mechanical property evaluation results of LipoGel (orange) and gel (blue). a) Storage modulus G' and viscous modulus G'' versus shear strains γ from rheology amplitude sweeps. b) Moduli G' and G'' versus frequency f from rheology frequency sweeps. c) The mean Young's modulus E values of the control alginate gel and LipoGels at 25C and 42 °C.

c_{ca2+} = 1 wt% to c_{ca2+} = 5 and 10 wt% led to a decrease in the mesh size from ξ = 11.3 ± 4.0 nm to ξ = 4.3 ± 0.4 and 1.0 ± 0.3 nm (cf. Table S6 in the Supporting Information), respectively, indicating additional cross-linking capacity at higher Ca^{2+} concentrations despite a similar water content S_w ≈80%.

The mesh size ξ characterizes the hydrogel nanostructure and is intimately related to the gel mechanical properties: a smaller mesh size indicates higher cross-linking density and a denser polymer network, leading to an enhanced gel mechanical strength,[46] as probed with rheology and microindentation measurements.

2.3. Mechanical Properties of LipoGels

Rheology measurements probed the viscoelastic behavior and mechanical properties of the alginate LipoGels. Both the control gel (no liposome) and LipoGel samples exhibited similar trends, from the amplitude (**Figure** 3a) and frequency (Figure 3b) sweeps, with the storage modulus G' and the loss modulus G'' of the control samples being slightly higher. The linear viscoelastic region for both gel types lies within the shear strain range γ = 0.01–0.15%, where the moduli remained independent of shear strain (Figure 3a). G' and G'' exhibited a plateau and remained

largely constant over the frequency sweep range $f = 0.1$–10 Hz performed at a shear strain of $\gamma = 0.1\%$ (Figure 3b), indicative of the mechanical stability of the alginate hydrogels across varying shear frequencies, desirable for practical applications.[47] The storage modulus G', characteristic of the elastic property, was consistently higher than the loss modulus G'', the viscous component, indicating that the hydrogel behaved predominantly like an elastic solid, as expected of hydrogels.

Notably, $G' \approx 200$ kPa is relatively high compared to the typical elastic moduli reported of alginate hydrogels cross-linked by Ca^{2+}, which generally range from 1 to 100 kPa.[27,48] For comparison, a pioneering cartilage-inspired chemically cross-linked poly(hydroxyethyl methacrylate) hydrogel system (also with liposomes incorporated) achieved an elastic modulus $G' \approx 50$ kPa.[16] The fourfold as high G' of the Ca^{2+} cross-linked alginate hydrogel presented here may be attributed to the slow thickening step of sodium alginate solutions before cross-linking in gel preparation (cf. Figure 1a), which served to enhance polymer centration, and in turn, the cross-linking density and gel rigidity. Importantly, the incorporation of DPPC liposomes did not compromise the mechanical strength of the hydrogel, in contrast to previously reported liposome-incorporating hydrogel systems.[16] While the amount of DPPC liposome added was relatively small (at a 0.08 wt% lipid concentration), the controlled gentle heating to allow homogenous thickening of the alginate–liposome solution (cf. Figure 1a) facilitated desired macroscopic gel properties, such as transparency, morphological consistency, and enhanced mechanical properties.

The mesh size ξ of the gel polymer network can also be estimated from the elastic modulus G' value as[49] $\xi = (6RT/\pi G' N_A)^{1/3}$, where R is the gas constant, T the absolute temperature, and N_A the Avogadro number. Using $G' \approx 200$ kPa from rheological measurements for the optimized hydrogel sample, we obtain $\xi \approx 3.40$ nm, consistent with the mesh size ξ of 3.60 ± 0.7 nm obtained from the SANS data (cf. Figure 2e).

A microindenter was used to further characterize the Young's modulus E of the hydrogels under water at 25 and 42 °C, below and above the DPPC tail phase transition temperature of 41.3 °C,[50] with the surface deformation modeled using the JKR theory of contact mechanics (cf. Section S1.2.8 in the Supporting Information). The Young's modulus E, reaching up to 1.08 ± 0.04 MPa, was higher than the storage modulus G' (up to 200 kPa). Young's modulus measures the stiffness of a material in response to uniaxial tensile or compressive stress in the linear elastic region,[51] while storage modulus G' obtained from a rheometer gauges the elastic component of a material's response to oscillatory shear deformation, characterizing the viscoelasticity.[52] As shown in Figure 3c, LipoGels displayed higher Young's moduli E at both temperatures than the control alginate gel; at 25 °C, its $E > 1$ MPa value significantly surpassed that of the control. This may be attributed to DPPC lipid hydration capacity facilitating stability against osmotic stress and the liposomes acting as elastic spheres fortifying the polymer network.

The lower Young's moduli E for the hydrogel at the higher temperature (i.e., 42 °C; cf. Figure 3c) is consistent with an earlier report, where the mechanical strength of Ca^{2+} cross-linked alginate hydrogels declined with increasing temperatures up to 50 °C.[53] Initially attributed to the rearrangement and breaking of weak junctions in the hydrogel,[53] the explanation was later revised to be related to the enthalpic elasticity behavior.[54]

For the LipoGel, DPPC would transition from the gel into the fluid phase at 42 °C, where its alkyl chains became disordered,[55] resulting in a mechanically less robust membrane[56] compared to the gel phase below the transition temperature, where the more rigid alkyl DPPC chains would adopt a more ordered arrangement.[57] Consequently, the reduction at 42 °C compared to 25 °C in Young's modulus E was more pronounced for the LipoGel, amounting to 25% compared to 17% for the control. Despite this, the DPPC-embedded hydrogel retained its robustness, with an average Young's modulus $E \approx 803.8 \pm 44.6$ kPa, highlighting the fortifying role of the liposomes in the physically cross-linked gel and underscoring its load-bearing capacity.

Furthermore, the tensile test was conducted to further characterize the mechanical properties of the LipoGels. As shown in Figure S14 in the Supporting Information, both the control gel (no liposomes) and the LipoGel from this study exhibited an ultimate tensile stress exceeding 1.5 MPa, in comparison to the typical value reported for Ca^{2+}–alginate hydrogels (below 40 kPa).[58] Notably, the LipoGel showed superior mechanical performance, reaching an ultimate stress of 2.40 ± 0.40 MPa, compared to 1.79 ± 0.03 MPa for the DPPC-free gel. These results are consistent with the mechanical trends observed in the indentation tests.

Compared to several representative Ca–alginate hydrogels from the literature, summarized in Table S7 in the Supporting Information, our preparation method is simpler and achieves superior mechanical properties relative to most physically cross-linked Ca–alginate hydrogels with elastic moduli G' generally below 100 kPa and Young's modulus E below 500 kPa.

2.4. Effective Lubrication Performance Evaluated through Tribology

The lubrication performance of the LipoGel was evaluated by measuring the CoF (μ) against a 8 mm stainless-steel ball under water using a UMT ball-on-disk tribometer at different loads (cf. Section S1.2.10 in the Supporting Information), compared to three types of alginate gel control samples: that without liposomes (labeled as "Gel" in **Figure 4**), that undergone shrinking (labeled as "Shrunk"), and that with DPPC aqueous dispersion sprayed onto the gel surface (labeled as "Sprayed"; cf. Figure S7c in the Supporting Information). As shown in Figure 4a, the shrunk hydrogel exhibited the poorest lubricity, with $\mu > 0.2$ across all the applied loads, pointing to the importance and benefit of morphological consistency in the gel preparation (cf. Figure 1a). The DPPC-sprayed sample demonstrated poorer lubrication performance than the DPPC-free sample. However, the LipoGel achieved the most effective lubrication, with $\mu < 0.05$ under all tested loads, with both the LipoGel and DPPC-free hydrogels reaching the ultralow friction region (i.e., $\mu < 0.1$).[59] While all the hydrogel samples displayed a consistent trend of increasing CoF with higher applied loads, the LipoGel exhibited superior performance, showing only a mild increase in CoF under higher loads (Figure 4e).

LipoGels incorporating DPPC ≈1000 nm MLVs or ≈100 nm SUVs were also compared. The sizes of 2 mM DPPC MLV and SUV solutions were measured by DLS, as shown in Figure S11 in

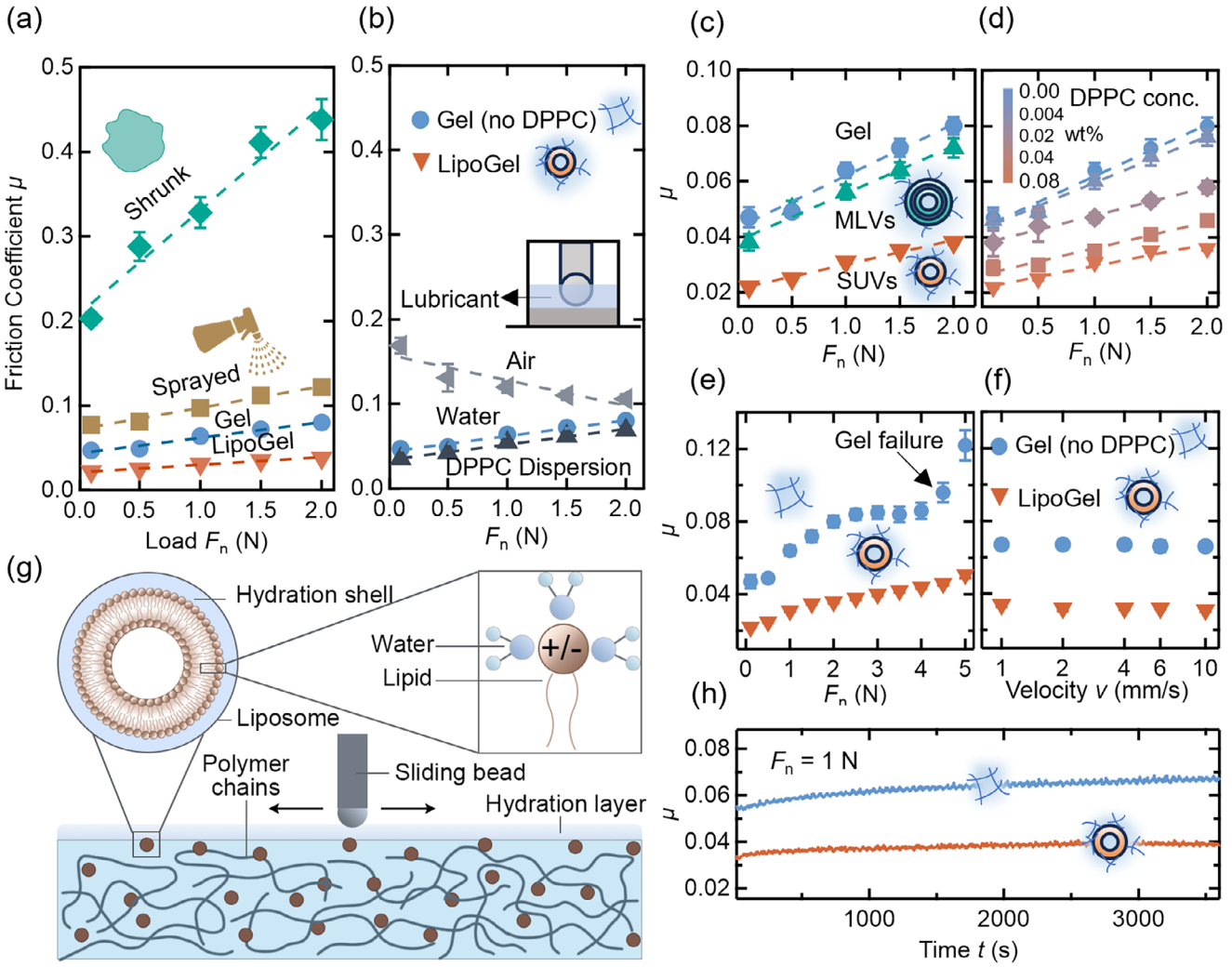

Figure 4. Lubrication characterization of LipoGels. Friction coefficient μ versus load F_n results for a) alginate hydrogels prepared using different methods; b) control DPPC-free gels under different conditions: in air, under water, and in 2 mM DPPC dispersion; c) LipoGels embedded with 0.08 wt% DPPC SUVs (≈100 nm in diameter) and MLVs (≈1000 nm in diameter); d) LipoGels embedded with different concentrations of DPPC SUVs; and e) the control DPPC-free gel and LipoGel (embedded with 0.08 wt% DPPC SUVs) in the higher normal load range at $v = 2$ mm s^{-1}. f) Friction coefficient (μ) versus shear velocity (v) under load $F_n = 1$ N. g) Schematic diagram of the lubricating mechanism of LipoGel. h) Comparison of μ monitored over a period of 1 h between the DPPC-free gel and LipoGel (with 0.08 wt% SUVs) at $F_n = 1$ N.

the Supporting Information. SANS analysis further revealed that the SUVs had a lipid bilayer thickness of ≈4.2 ± 0.1 nm and a diameter of ≈88 ± 2.2 nm, while confirming the formation of MLVs with a peak position at 0.10 Å^{-1} corresponding to a *d*-spacing of 62.8 Å (cf. Section S14 in the Supporting Information).[60] As shown in Figure 4c, the SUV LipoGel exhibited the lowest CoF, while the MLV LipoGel facilitated slightly better lubrication compared to the control sample. The larger size and broader size distribution of MLVs resulted in clustering and an inhomogeneous distribution within the hydrogel matrix (cf. Figure 2c). By contrast, smaller SUVs were more uniformly distributed across the hydrogel (cf. Figure 2d), facilitating more homogeneous hydration and imparting fortification to the gel mechanical robustness (cf. Figure 3c), also mediating more effective lubrication.

The effect of the lipid concentration on lubrication was examined on LipoGels embedded with different amounts of DPPC liposomes under the optimized gelation conditions. As shown in Figure 4d, the CoF decreased as the lipid concentration increased, with the LipoGel exhibiting improved lubrication performance at higher lipid concentrations. Remarkably, even a trace amount of DPPC liposomes, at a lipid concentration of 0.08 wt% (derived from adding 1 mL of 2 mM DPPC liposomes), reduced CoF from $\mu = 0.047 \pm 0.004$ to $\mu = 0.022 \pm 0.001$ at a normal load of $F_n = 0.1$ N, with the lubrication improvement even more pronounced at higher loads. As schematically illustrated in Figure 4g, the exceptional hydration capability of DPPC liposomes underpins their impact on the improved lubricating capability of LipoGels.[5c] The highly hydrated zwitterionic DPPC lipid head groups can create a tenaciously bound hydration layer, which plays a key role in the hydration lubrication mechanism.[6a] As Lin et al. have explained,[16] the lubricious hydrated liposome headgroups at the hydrogel boundary are in contact with the opposing sliding

object, rather than the hydrogel surface itself. Sliding against the water film on the elastic hydrogel material not only reduces friction but also effectively dissipates energy from the applied load. With more liposomes incorporated, one would expect more effective hydration at the hydrogel boundary, mediating more effective lubrication.

Such importance of the interfacial hydration at the hydrogel boundary layer was demonstrated by comparing the CoF of the alginate gel in air, water, and a 2 mM DPPC SUV dispersion. As shown in Figure 4b, the gel exhibited certain lubrication efficacy in air ($\mu = 0.170 \pm 0.009$ at $F_n = 0.1$ N) due to the relatively high water content ($S_w \approx 80\%$), and the reduction in CoF with load in air may be attributed to water being expelled from the hydrogel matrix of the surface. In comparison, submission in water and the DPPC dispersion led to appreciable improvement in its lubrication performance, albeit the LipoGel with embedded liposomes mediated the most effective lubrication. It is conceivable that the weak anchoring of liposomes from the solution onto the hydrogel surface would limit their effectiveness to hydration boundary lubrication, particularly at higher loads.

Lubrication performance of the LipoGel (embedded with 0.08 wt% DPPC SUVs) was also benchmarked against the control DPPC-free gel over a wider load range ($F_n \approx 0$–5 N). As shown in Figure 4e, the LipoGel CoF increased gradually from $\mu = 0.022 \pm 0.001$ to $\mu = 0.051 \pm 0.002$, remaining within the ultralow friction regime. A higher load would result in more pronounced elastic hydrogel deformation at the contact and increased friction associated with a larger contact area, and also overcoming the resistance from the deformation upon sliding.[61] By contrast, the DPPC-free hydrogel sustained a CoF approximately twice as high up to load $F_n \approx 4$ N, at which μ experienced a marked rise attributed to possible local structural disruption to the polymer network. Such a more superior loadbearing capacity by the LipoGel while maintaining effective lubrication is consistent with its higher Young's modulus from microindentation measurement (i.e., $E \approx 1.1$ MPa at 25 °C; cf. Figure 3c) compared to the DPPC-free gel ($E \approx 700$ kPa).

The CoF of the hydrogels also appeared independent of sliding velocity within the range of 1–10 mm s^{-1} (evaluated at $F_n \approx 1$ N; Figure 4f). The lubrication longevity of the hydrogels was tested over 60 min under water at $F_n = 1$ N. As shown in Figure 4h, LipoGel maintained a CoF of $\mu \approx 0.038$ over the period; by contrast, the control sample exhibited a noticeable increase in CoF in the first 1000 s, followed by a gradual rise over time.

3. Further Discussions and Concluding Remarks

Concentrating alginate solutions before cross-linking via controlled evaporation has proven to be a simple and effective method for resolving the shrinkage issue in gelation by divalent cation cross-linking. This approach overcomes the practical challenges of slow solubility and high solution viscosity at high alginate concentrations. It also eliminates bubble generation commonly experienced during mechanical stirring or mixing, enabling reproducible fabrication of a transparent, homogeneous hydrogel with morphological consistency. Resolving the common shrinkage-upon-gelation problem ultimately enhanced the hydrogel's structural consistency and mechanical strength, enabling its use as a load-bearing material.

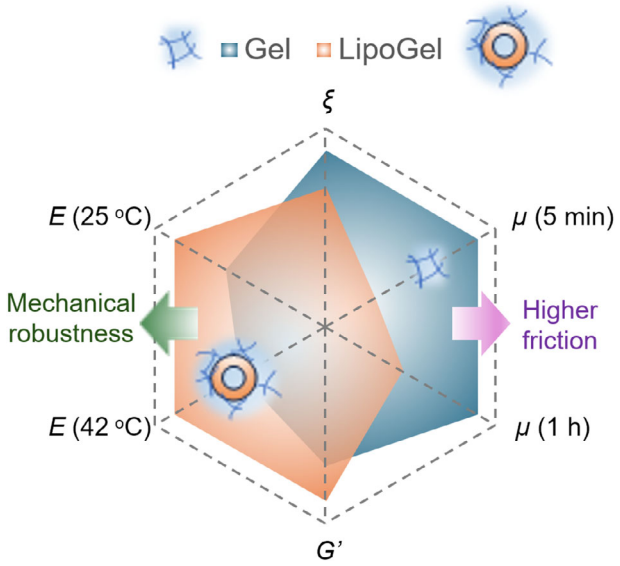

Figure 5. Radar chart of the nanostructural, lubrication, and mechanical property profile, giving an overview of the relative differences between LipoGel (orange) and Gel (blue; no liposomes) in the following parameters: friction coefficient μ at the load of $F_n = 1$ N after 5 min and 1 h from tribology, Young's modulus E from indentation at 25 and 42 °C, viscoelastic modulus G' from rheology, and mesh size ξ from SANS, with the control gel (no liposomes) showing higher friction while LipoGel exhibited higher mechanical robustness evident from higher E and G' values. In plotting the chart, which appears as a hexagon with six dimensionless axes/spokes all on a scale of 0–1, each of the six parameters is normalized with respect to the maximum values registered across the two gel types.

While recent development of double-network or bilayer hydrogels has achieved exceptionally high contact pressure (approaching several MPa),[62] these systems require complex synthesis processes with multiple chemical ingredients, steps, and reaction conditions to be optimized, posing challenges for facile gel preparation and also biocompatibility. Physical cross-linking through simple Ca^{2+} addition here—via a controlled concentrating step—achieved a robust LipoGel with a shear elastic modulus G' 4 times that of a chemically cross-linked hydrogel incorporating liposomes,[16] with the Young's modulus ($E \approx 1$ MPa) comparable to some of the recent chemically cross-linked hydrogels (such as the double network—agarose and poly(acrylamide and acrylic acid) hydrogel[63] and micropored poly(2-hydroxyethyl methacrylate) hydrogel)[64] designed for lubrication. It thus offers a more accessible and practical route for hybrid functional LipoGel synthesis.

The radar chart in **Figure 5** gives an overview of the relative differences and correlation between different parameters characterizing the nanostructural (mesh size ξ), lubrication (friction coefficient μ), and the mechanical properties (Young's modulus E and shear elastic modulus G') of LipoGel and the control gel (no liposomes). Overall, LipoGel demonstrated more effective lubrication performance and more robust mechanical properties. Alginate hydrogels are intrinsically self-lubricious in water, achieving a coefficient of friction $\mu < 0.1$. The incorporation of trace amounts of DPPC liposomes (SUVs) in this work, inspired by an approach pioneered by Klein and co-workers incorporating MLVs in a chemically cross-linked hydrogel,[16] significantly

improved lubricity, reducing μ to as low as 0.02—comparable to that of advanced lubricating hydrogels reported in recent studies.[10a] With liposomes extensively employed as drug-delivery vectors,[65] their integration into the hydrogel matrix opens up the possibility for multifunctional therapeutic biolubricants. The successful encapsulation of a hydrophobic fluorescent dye in DPPC liposomes incorporated in the gel in this study serves as proof of concept, demonstrating the potential for encapsulating and delivering therapeutic agents such as anti-inflammatory drugs. In this context, biocompatibility is a crucial consideration for hydrogels intended for biomedical applications. Numerous previous studies have validated the biocompatibility of alginate-based hydrogels, including cell viability assays showing their minimal cytotoxicity.[66] Furthermore, DPPC as a key component of mammalian cell membranes, is also prominent in the synovial fluid,[67] making it inherently biocompatible and noncytotoxic.

In conclusion, a liposome-embedded hydrogel (LipoGel) has been successfully developed using the naturally derived biomaterial alginate and a simple physical cross-linking method. The critical issue of shrinkage upon gelation was effectively resolved by concentrating the alginate solution to 6.7 wt% before cross-linking. The optimized cross-linking conditions were determined using water content as an index, including the drying time, cross-linking time ($t_{cl} \approx 30$ min), and Ca^{2+} concentration ($c_{Ca2+} \approx 5$ wt%), giving a gel water content of $S_w \approx 80\%$. Confocal fluorescent microscopy confirmed the uniform distribution of DPPC (SUV) liposomes within the hydrogel matrix, while cryo-SEM revealed a compact porous structure with an average pore size of ≈92 nm and also clear visualization of individual liposomes embedded within the polymer network. The nanostructure of the hydrogels was probed using SANS, and their mechanical properties were examined through rheological and microindentation measurements. The LipoGel exhibited a storage modulus $G' \approx$ 200 kPa and a mesh size of $\xi \approx 3.5$ nm, consistently ascertained from SANS and rheology measurements. The incorporation of DPPC liposomes fortified the gel Young's modulus, with microindentation yielding $E \approx 1$ MPa at 25 °C for the LipoGel compared to $E \approx 700$ kPa for the control alginate gel. The lubrication performance of the LipoGels was critically compared with control gel samples. The results show that alginate LipoGel embedded with only 0.08 wt% DPPC liposomes achieved a low friction coefficient of $\mu \approx 0.021$ under a pressure of 0.45 MPa. The LipoGels also sustained superior lubrication efficacy, compared to controls, under higher loads, which is insensitive to sliding velocity. LipoGels developed in this study combine a simple chemical composition with a facile preparation method. Its enhanced mechanical strength, superior lubricity, and potential for therapeutic encapsulation, coupled with strong biocompatibility, make it a promising material for future research and practical use. The transparency of the LipoGels would also permit ready light access to the gel interior for potential noninvasive activation of therapeutic actives, an aspect that remains to be further explored. It would also be interesting to evaluate the frictional behavior of LipoGels under different conditions, such as elevated temperatures and pressures and evaluate the wear resistance of the gels.

Supporting Information

Supporting Information is available from the Wiley Online Library or from the author.

Acknowledgements

T.M. was supported by the China Scholarship Council (CSC)–University of Bristol (UoB) Ph.D. Scholarship. The authors gratefully acknowledge the Science and Technology Facilities Council (STFC) for access to the neutron beamtime at ISIS at the SANS2D instrument (Grant No. RB2320068) and the staff there for their help. The authors also would like to thank Magdalena Włodek, Matteo Fois, Sofia Rogers Ruiz, and Oliver McDowell for their assistance with the SANS experiment. Data obtained at ISIS are available at; https://doi.org/10.5286/ISIS.E.RB2320068. The authors also gratefully acknowledge the Wolfson Bioimaging Facility for their support and assistance with the cryo-SEM imaging and confocal microscopy. Several icons were created in BioRender with the license granted to T.M. (2025) https://BioRender.com/8rgi6d3.

Conflict of Interest

The authors declare no conflict of interest.

Author Contributions

T.M.: investigation, methodology, data curation, formal analysis, software, validation, visualization, writing—original draft. X.G.: methodology, data curation, writing—review and editing. N.M.: methodology, data curation, software. P.G.: methodology, validation, writing—review and editing. W.H.B.: conceptualization, supervision, methodology, funding acquisition, validation, visualization, writing—review and editing.

Data Availability Statement

The data that support the findings of this study are available from the corresponding author upon reasonable request.

Keywords

alginate gels, biomimetic lubrication, hydrogels, LipoGels, liposomes, SANS

Received: June 9, 2025
Revised: July 21, 2025
Published online:

[1] H. Forster, J. Fisher, *Proc. Inst. Mech. Eng., Part H* **1996**, *210*, 109.
[2] W. A. Hodge, R. S. Fijan, K. L. Carlson, R. G. Burgess, W. H. Harris, R. W. Mann, *Proc. Natl. Acad. Sci. USA* **1986**, *83*, 2879.
[3] W. H. Briscoe, *Curr. Opin. Colloid Interface Sci.* **2017**, *27*, 1.
[4] a) L. Zhou, V. O. GJVM, J. Malda, M. J. Stoddart, Y. Lai, R. G. Richards, K. Ki-wai Ho, L. Qin, *Adv. Healthcare Mater.* **2020**, *9*, 2001008; b) W. Lin, J. Klein, *Adv. Mater.* **2021**, *33*, 2005513.
[5] a) G. Ateshian, *J. Biomech. Eng.* **1997**, *119*, 81; b) D. Dowson, *Faraday Discuss.* **2012**, *156*, 9; c) J. Seror, L. Zhu, R. Goldberg, A. J. Day, J. Klein, *Nat. Commun.* **2015**, *6*, 6497.

[6] a) J. Klein, *Friction* **2013**, *1*, 1; b) S. Jahn, J. Seror, J. Klein, *Annu. Rev. Biomed. Eng.* **2016**, *18*, 235.
[7] U. Raviv, J. Klein, *Science* **2002**, *297*, 1540.
[8] A. Sarma, G. Powell, M. LaBerge, *J. Orthop. Res.* **2001**, *19*, 671.
[9] a) M. Chen, W. H. Briscoe, S. P. Armes, J. Klein, *Science* **2009**, *323*, 1698; b) F. Foglia, M. J. Lawrence, C. D. Lorenz, S. E. McLain, *J. Chem. Phys.* **2010**, *133*, 145103.
[10] a) W. Lin, J. Klein, *Acc. Mater. Res.* **2022**, *3*, 213; b) W. Li, J. Lai, Y. Zu, P. Lai, *Innovation* **2022**, *3*, 100275.
[11] E. M. Ahmed, *J. Adv. Res.* **2015**, *6*, 105.
[12] X. Liu, J. Liu, S. Lin, X. Zhao, *Mater. Today* **2020**, *36*, 102.
[13] a) O. Wichterle, D. LÍM, *Nature* **1960**, *185*, 117; b) C. M. Beddoes, M. R. Whitehouse, W. H. Briscoe, B. Su, *Materials* **2016**, *9*, 443.
[14] a) S. M. McNary, K. A. Athanasiou, A. H. Reddi, *Tissue Eng., Part B* **2012**, *18*, 88; b) C. Qin, H. Yang, Y. Lu, B. Li, S. Ma, Y. Ma, F. Zhou, *Adv. Mater.* **2025**, 2420626.
[15] K. Wang, Q. Ma, Y.-M. Zhang, G.-T. Han, C.-X. Qu, S.-D. Wang, *Cellulose* **2020**, *27*, 1845.
[16] W. Lin, M. Kluzek, N. Iuster, E. Shimoni, N. Kampf, R. Goldberg, J. Klein, *Science* **2020**, *370*, 335.
[17] M. Qu, H. Liu, C. Yan, S. Ma, M. Cai, Z. Ma, F. Zhou, *Chem. Mater.* **2020**, *32*, 7805.
[18] Y.-S. Pan, D.-S. Xiong, R.-Y. Ma, *Wear* **2007**, *262*, 1021.
[19] W. E. Hennink, C. F. van Nostrum, *Adv. Drug Delivery Rev.* **2012**, *64*, 223.
[20] a) J. Yang, Y. Chen, L. Zhao, J. Zhang, H. Luo, *Polym. Rev.* **2023**, *63*, 574; b) X. Xue, Y. Hu, S. Wang, X. Chen, Y. Jiang, J. Su, *Bioact. Mater.* **2022**, *12*, 327.
[21] Z. Gong, G. Zhang, X. Zeng, J. Li, G. Li, W. Huang, R. Sun, C. Wong, *ACS Appl. Mater. Interfaces* **2016**, *8*, 24030.
[22] L. Zhang, W. Ma, H. Tang, Y. Yu, L. Wang, T. Li, Z. Fang, Z. Qiao, *Chem. Eng. J.* **2023**, *466*, 143195.
[23] O. Smidsrød, G. Skja, *Trends Biotechnol.* **1990**, *8*, 71.
[24] M. B. Łabowska, A. M. Jankowska, I. Michalak, J. Detyna, *Key Eng. Mater.* **2021**, *885*, 39.
[25] D. Massana Roquero, A. Othman, A. Melman, E. Katz, *Mater. Adv.* **2022**, *3*, 1849.
[26] R. Hassan, F. Tirkistani, I. Zaafarany, A. Fawzy, M. Khairy, S. Iqbal, *Adv. Biosci. Biotechnol.* **2012**, *3*, 845.
[27] H. Malektaj, A. D. Drozdov, J. deClaville Christiansen, *Polymers* **2023**, *15*, 3012.
[28] D. Ji, J. M. Park, M. S. Oh, T. L. Nguyen, H. Shin, J. S. Kim, D. Kim, H. S. Park, J. Kim, *Nat. Commun.* **2022**, *13*, 3019.
[29] S. Nakajima, R. Kawano, H. Onoe, *Soft Matter* **2017**, *13*, 3710.
[30] a) J. Zhao, Y. Wang, C. Liu, *Food Anal. Methods* **2022**, *15*, 2840; b) L. Han, L. Yan, M. Wang, K. Wang, L. Fang, J. Zhou, J. Fang, F. Ren, X. Lu, *Chem. Mater.* **2018**, *30*, 5561.
[31] a) S. F. bt Ibrahim, N. A. N. Mohd Azam, K. A. Mat Amin, *IOP Conf. Ser.: Mater. Sci. Eng.* **2019**, *509*, 012063; b) W.-P. Voo, C.-W. Ooi, A. Islam, B.-T. Tey, E.-S. Chan, *Eur. Polym. J.* **2016**, *75*, 343.
[32] P.-G. De Gennes, *Scaling Concepts in Polymer Physics*, Cornell University Press, Ithaca and London **1979**.
[33] Y. Gao, N. K. Chai, N. Garakani, S. S. Datta, H. J. Cho, *Soft Matter* **2021**, *17*, 9893.
[34] Y. Guo, J. Bae, Z. Fang, P. Li, F. Zhao, G. Yu, *Chem. Rev.* **2020**, *120*, 7642.
[35] G. T. Grant, E. R. Morris, D. A. Rees, P. J. Smith, D. Thom, *FEBS Lett.* **1973**, *32*, 195.
[36] R. Aston, K. Sewell, T. Klein, G. Lawrie, L. Grøndahl, *Eur. Polym. J.* **2016**, *82*, 1.
[37] S. Liu, H. Li, B. Tang, S. Bi, L. Li, *Carbohydr. Polym.* **2016**, *135*, 101.
[38] N. G. Zhegalova, S. He, H. Zhou, D. M. Kim, M. Y. Berezin, *Contrast Media Mol. Imaging* **2014**, *9*, 355.
[39] B. Hammouda, D. L. Ho, S. Kline, *Macromolecules* **2004**, *37*, 6932.
[40] B. Hammouda, D. Ho, S. Kline, *Macromolecules* **2002**, *35*, 8578.
[41] N. A. Peppas, P. Bures, W. Leobandung, H. Ichikawa, *Eur. J. Pharm. Biopharm.* **2000**, *50*, 27.
[42] E. M. Saffer, M. A. Lackey, D. M. Griffin, S. Kishore, G. N. Tew, S. R. Bhatia, *Soft Matter* **2014**, *10*, 1905.
[43] a) L. G. B. Bremer, B. H. Bijsterbosch, P. Walstra, T. van Vliet, *Adv. Colloid Interface Sci.* **1993**, *46*, 117; b) S. E. S. Michel, S. E. Rogers, W. H. Briscoe, M. C. Galan, *ACS Appl. Bio Mater.* **2020**, *3*, 8075.
[44] S. Morariu, C. E. Brunchi, M. Cazacu, M. Bercea, *J. Chem. Eng. Data* **2011**, *56*, 1468.
[45] R. Zhang, P. Lin, W. Yang, M. Cai, B. Yu, F. Zhou, *Polym. Chem.* **2017**, *8*, 7102.
[46] Z. K. Zander, G. Hua, C. G. Wiener, B. D. Vogt, M. L. Becker, *Adv. Mater.* **2015**, *27*, 6283.
[47] K. Ghosh, X. Z. Shu, R. Mou, J. Lombardi, G. D. Prestwich, M. H. Rafailovich, R. A. F. Clark, *Biomacromolecules* **2005**, *6*, 2857.
[48] a) M. Matyash, F. Despang, C. Ikonomidou, M. Gelinsky, *Tissue Eng., Part C* **2014**, *20*, 401; b) J. Jang, Y.-J. Seol, H. J. Kim, J. Kundu, S. W. Kim, D.-W. Cho, *J. Mech. Behav. Biomed. Mater.* **2014**, *37*, 69.
[49] a) P. J. Flory, *Principles of Polymer Chemistry*, Cornell University Press, New York **1953**; b) L. Pescosolido, L. Feruglio, R. Farra, S. Fiorentino, I. Colombo, T. Coviello, P. Matricardi, W. E. Hennink, T. Vermonden, M. Grassi, *Soft Matter* **2012**, *8*, 7708.
[50] R. L. Biltonen, D. Lichtenberg, *Chem. Phys. Lipids* **1993**, *64*, 129.
[51] H. E. Symons, A. Galanti, J. C. Surmon, R. S. Trask, S. Rochat, P. Gobbo, *Soft Matter* **2022**, *18*, 8302.
[52] N. Chandran, C. Sarathchandran, S. Thomas, in *Rheology of Polymer Blends and Nanocomposites*, Elsevier, Amsterdam **2020**, pp. 1–17.
[53] I.-L. Andresen, O. Smidsørod, *Carbohydr. Res.* **1977**, *58*, 271.
[54] S. T. Moe, K. I. Draget, G. Skjåk-Bræk, O. Simdsrød, *Carbohydr. Polym.* **1992**, *19*, 279.
[55] K. A. Riske, R. P. Barroso, C. C. Vequi-Suplicy, R. Germano, V. B. Henriques, M. T. Lamy, *Biochim. Biophys. Acta, Biomembr.* **2009**, *1788*, 954.
[56] N. Michel, A.-S. Fabiano, A. Polidori, R. Jack, B. Pucci, *Chem. Phys. Lipids* **2006**, *139*, 11.
[57] R. M. Venable, F. L. H. Brown, R. W. Pastor, *Chem. Phys. Lipids* **2015**, *192*, 60.
[58] J. L. Drury, R. G. Dennis, D. J. Mooney, *Biomaterials* **2004**, *25*, 3187.
[59] J. Shi, W. Wang, J. Yang, X. Cao, J. Zhang, C. Wang, *Tribol. Int.* **2021**, *154*, 106746.
[60] M.-P. Nieh, C. J. Glinka, S. Krueger, R. S. Prosser, J. Katsaras, *Biophys. J.* **2002**, *82*, 2487.
[61] L. Gao, X. Zhao, S. Ma, Z. Ma, M. Cai, Y.-M. Liang, F. Zhou, *Friction* **2022**, *10*, 1046.
[62] X. Zhao, W. Zhao, Y. Zhang, X. Zhang, Z. Ma, R. Wang, Q. Wei, S. Ma, F. Zhou, *Biosurf. Biotribol.* **2022**, *8*, 225.
[63] M. J. Lee, R. M. Espinosa-Marzal, *ACS Appl. Mater. Interfaces* **2023**, *15*, 20495.
[64] Y. Xi, P. K. Sharma, H. J. Kaper, C.-H. Choi, *ACS Appl. Mater. Interfaces* **2021**, *13*, 41473.
[65] Y. Liu, K. M. C. Bravo, J. Liu, *Nanoscale Horiz.* **2021**, *6*, 78.
[66] a) S. Li, X. Wang, J. Chen, J. Guo, M. Yuan, G. Wan, C. Yan, W. Li, H.-G. Machens, Y. Rinkevich, X. Yang, H. Song, Z. Chen, *Int. J. Biol. Macromol.* **2022**, *202*, 657; b) Y. Han, Q. Zeng, H. Li, J. Chang, *Acta Biomater.* **2013**, *9*, 9107; c) E. A. Nunamaker, E. K. Purcell, D. R. Kipke, *J. Biomed. Mater. Res., Part A* **2007**, *83*, 1128.
[67] M. K. Kosinska, G. Liebisch, G. Lochnit, J. Wilhelm, H. Klein, U. Kaesser, G. Lasczkowski, M. Rickert, G. Schmitz, J. Steinmeyer, *Arthritis Rheum.* **2013**, *65*, 2323.